

See discussions, stats, and author profiles for this publication at: <https://www.researchgate.net/publication/264636869>

Structure and Aggregation in the 1,3-dialkyl-imidazolium Bis(Trifluoromethylsulfonyl)Imide Ionic Liquid Family. 2. From Single to Double Long Alkyl Side Chains.

ARTICLE *in* THE JOURNAL OF PHYSICAL CHEMISTRY B · MAY 2014

Impact Factor: 3.3 · DOI: 10.1021/jp502968u · Source: PubMed

CITATIONS

14

READS

34

5 AUTHORS, INCLUDING:



Carlos E S Bernardes

Centro de Química e Bioquímica, Faculdade d...

47 PUBLICATIONS 496 CITATIONS

[SEE PROFILE](#)



Ana I M C Lobo Ferreira

University of Porto

45 PUBLICATIONS 469 CITATIONS

[SEE PROFILE](#)



Luís M N B F Santos

University of Porto

237 PUBLICATIONS 3,693 CITATIONS

[SEE PROFILE](#)



Jose Nuno A Canongia Lopes

Technical University of Lisbon

179 PUBLICATIONS 8,341 CITATIONS

[SEE PROFILE](#)

Structure and Aggregation in the 1,3-Dialkyl-imidazolium Bis(trifluoromethylsulfonyl)imide Ionic Liquid Family: 2. From Single to Double Long Alkyl Side Chains

Carlos E. S. Bernardes,[†] Karina Shimizu,^{†,‡} Ana I. M. C. Lobo Ferreira,^{†,§} Luís M. N. B. F. Santos,[§] and José N. Canongia Lopes^{*,†,‡}

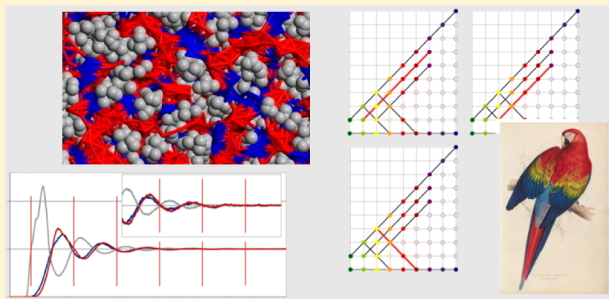
[†]Centro de Química Estrutural, Instituto Superior Técnico, Universidade de Lisboa, Av. Rovisco Pais, 1049-001 Lisboa, Portugal

[‡]Instituto de Tecnologia Química e Biológica, Universidade Nova de Lisboa, Av. República, 2780-157 Oeiras, Portugal

[§]Centro de Investigação em Química, Departamento de Química e Bioquímica, Faculdade de Ciências da Universidade do Porto, R. Campo Alegre 687, P-4169-007 Porto, Portugal

Supporting Information

ABSTRACT: A systematic molecular dynamics study using large simulation boxes has been performed in order to extend the analysis of the mesoscopic segregation behavior observed in ionic liquids of the 1,3-dialkyl-imidazolium bis(trifluoromethylsulfonyl)imide homologous series, $[C_nC_m\text{im}][\text{Ntf}_2]$ ($2 \leq n \leq 10$, $2 \leq m \leq n$). The analyses include the discussion of the structure factors, $S(q)$, in the low- q range ($1.6 \leq q/\text{nm}^{-1} \leq 20$); the confirmation of the periodicity of the polar network of the ionic liquid and its relation to the so-called intermediate peaks; and the characterization of the polar network and the nonpolar regions that are formed along the series using aggregate analyses by means of five different statistical tools. The analyses confirmed that the percolation of the nonpolar regions into a continuous domain occurs when the total number of carbon atoms in the alkyl chains exceeds six but that this is not a sufficient condition for the emergence of a distinct and intense prepeak. The existence of such a peak also requires that the longer alkyl chain contains more than a critical alkyl length (CAL) of five carbon atoms.



INTRODUCTION

Ionic liquids are complex fluids whose structure on the molecular scale has been investigated in the past decade using both experimental and theoretical methodologies.^{1–18}

Recently we have further explored the relation between the nature of the ions that compose ionic liquids and their structure by performing systematic molecular dynamics simulations on the well-known 1-alkyl-3-methylimidazolium bistriflamide, $[C_nC_1\text{im}][\text{Ntf}_2]$, homologous series.¹⁹ The gradual lengthening of the single alkyl side chain along this family of ionic liquids allowed us to confirm the link between the nanosegregated structure of ionic liquids and the appearance of the so-called prepeaks in the corresponding structure-factor spectra (obtained both by simulation and experimentally). Such mesoscopic structures, composed of a polar network permeated by nonpolar regions, were also probed via the analysis of the so-called intermediate peaks of the structure-factor spectra—a measure of the spatial periodicity of the polar network—and through the introduction of several statistical tools adequate for the description of different aggregation parameters related to the morphology of the coexisting polar and nonpolar domains.

In this article, we extend such studies on the mesoscopic structure of ionic liquids to encompass other 1,3-dialkylmethylimidazolium bistriflamide homologous series, $[C_nC_m\text{im}]$

$[\text{Ntf}_2]$, including those with cations substituted by symmetrical alkyl side chains.

EXPERIMENTAL SECTION

Ionic Liquid Systems. Scheme 1 shows the relationships between the $[C_nC_m\text{im}][\text{Ntf}_2]$ ionic liquids studied in this work by arranging them in an array with all possible alkyl side chain combinations with $1 \leq n \leq 10$ and $1 \leq m \leq 10$.

The five studied homologous series include (i) alkyl side chains of the same length (symmetrical cations), $[C_nC_m\text{im}][\text{Ntf}_2]$ ($m = n$); (ii) chains that differ by one methylene group, $[C_nC_{m+1}\text{im}][\text{Ntf}_2]$ ($m = n - 1$); (iii) chains that differ by two methylene groups, $[C_nC_{m+2}\text{im}][\text{Ntf}_2]$ ($m = n - 2$); (iv) chains with a total of six carbon atoms, $[C_nC_{m+3}\text{im}][\text{Ntf}_2]$ ($n + m = 6$); and (v) chains with a total of eight carbon atoms, $[C_nC_{m+4}\text{im}][\text{Ntf}_2]$ ($n + m = 8$). Vignettes of Scheme 1 are introduced as small insets in most figures in order to highlight the series under discussion.

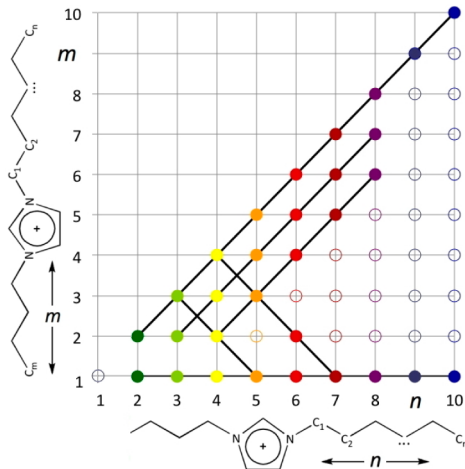
Molecular Dynamics Simulation. All $[C_nC_m\text{im}][\text{Ntf}_2]$ systems were modeled using the CL&P atomistic force

Received: March 25, 2014

Revised: May 29, 2014

Published: May 29, 2014

Scheme 1. Schematic Representation Showing Different Homologous Series of 1,3-Dialkyl-imidazolium Bistriflamide, $[C_n C_m im][Ntf_2]$, Ionic Liquids^a



^aThe five solid lines in bold and corresponding filled circles represent series studied in this work; the thin line represents a previously studied series.¹⁹ The color scheme distinguishes between cations with alkyl side chains of different lengths (longest chain).

field,^{20–22} which is an extension of the AMBER and OPLS force fields²³ specially designed to study ionic liquids and their homologous series.

Molecular dynamics simulations were carried out using the DL_POLY 2.20 package.²⁴ The runs were performed with a 2 fs time step and a 2 nm cutoff distance. Ewald summation corrections were performed beyond the cutoffs.

Two sets of simulations were performed. The first set comprised simulation cubic boxes with 300 ion pairs of each ionic liquid. All simulations started from low-density configurations that were subjected to equilibration runs under isobaric isothermal ensemble conditions ($p = 0.1$ MPa and $T = 400$ K with Nosé–Hoover thermostats and barostats with relaxation time constants of 1 and 4 ps, respectively). After 1.3 ns, the density of each system reached constant and consistent values, indicating that equilibrium had been attained and possible ergodicity problems had been overcome. Finally, several (at least four) consecutive production stages of 1.0 ns each were performed, and the combined results were used for the structural and aggregation analyses of all studied ionic liquids (see below). The second set of simulations used simulation boxes composed of 2400 ion pairs. These boxes were created by stacking eight equilibrated boxes from the first set in order to generate $2 \times 2 \times 2$ simulation boxes. The initial configurations thus obtained were then re-equilibrated/relaxed for 0.3 ns at $p = 0.1$ MPa, $T = 1000$ K. This was followed by several consecutive (at least 10) production stages of 0.1 ns each at $p = 0.1$ MPa and $T = 400$ K. These larger boxes and corresponding production data were used to calculate $g(r)$ functions in the $[C_n C_m im][Ntf_2]$ series, with $n = m = 2, 4, 6$, and 8.

Structural Analyses. The pair radial distribution functions $g_{ij}(r)$ between selected pairs of atoms or interaction centers were calculated in the usual way.²⁵ In the case of a few systems, these were calculated using large simulation boxes (cf. previous paragraph) that allowed the calculation of the corresponding $g_{ij}(r)$ functions up to distances of at least $r = 5.0$ nm. Otherwise, the $g_{ij}(r)$ functions were calculated up to $r = 2.5$ nm.

The total static structure factors, $S(q)$, were calculated using a previously described methodology.²⁶ In brief, $S(q)$ was obtained from

$$S(q) = \sum_i \sum_j S_{ij}(q) \quad (1)$$

$$S_{ij}(q) = \frac{\rho_o x_i x_j(q) b_j(q) \int_0^R 4\pi r^2 [g_{ij}(r) - 1] \frac{\sin(qr)}{qr} \frac{\sin(\pi R)}{\pi r / R} dr}{(\sum_i x_i b_i(q))^2} \quad (2)$$

where $S_{ij}(q)$ is the partial static structure factor between atoms of type i and j (e.g., carbon, hydrogen, or nitrogen), calculated from the corresponding Fourier transform of the partial radial distribution function $g_{ij}(r)$; q is the scattering vector; ρ_o is the average atom number density; R is the cutoff used in the calculation of $g_{ij}(r)$, established to half the side of the simulation box (in this case at least 5.2 nm for any of the studied ionic liquids); x_i and x_j are the atomic fractions of i and j ; and $b_i(q)$ and $b_j(q)$ are the coherent bound neutron scattering lengths of the corresponding atom type, interpolated from recommended values in the International Tables for Crystallography.²⁷ The term $\sin(\pi R)/(qr/R)$ in eq 2 is a Lorch-type window function used to reduce the effect of using a finite cutoff in the radial distribution function calculation.²⁸

Aggregation Analysis. The aggregation analyses of the $[C_n C_m im][Ntf_2]$ ionic liquids focused on two types of issues: (i) the evaluation of the connectivity between the charged moieties of the molecular ions that compose the so-called polar network and (ii) the calculation of the connectivity between the alkyl side chains and an estimation of the aggregate size/shape of the corresponding nonpolar domains.

The connectivity analyses of either the polar moieties that compose the polar network or the alkyl chains that form the nonpolar aggregates are based on previously described algorithms^{19,29} that generate neighbor lists of interaction centers of a given type in a three-stage sequential process.

First, the different types of interaction centers are defined: the center of mass of the imidazolium ring, “im”, and the nitrogen atom of the bistriflamide anion, NBT, in the case of the charged moieties; the C2 to CT (cf. Scheme 1) carbon atoms in the case of the alkyl chains.

Second, a connectivity threshold for each case is established by considering the corresponding $g_{ij}(r)$ data.¹⁹ Within the polar network the im–NBT interionic distance has been set to 0.8 nm, corresponding to the first coordination shell limit of the $g_{ij}(r)$ data; in the case of the alkyl side chains, the threshold has been set at 0.5 nm for the distance between any of the C2 to CT atoms belonging to two different alkyl chains. This also corresponds to contact distances taken from the relevant $g_{ij}(r)$ data.¹⁹

Third, the use of the threshold criteria allows the computation of closest-neighbor lists for each interaction center for all recorded configurations in the production runs, thus ascertaining the connectivity within the polar network or the nonpolar domains. In the case of the polar network, the connectivity is stipulated as always being between ions of opposite sign (cations connected to anions and vice versa); in the nonpolar domains the original programs, where chains are considered to belong to the same aggregate if the distance between any two carbon atoms of the two chains is lower than 0.5 nm, were modified in order to ensure that the two alkyl chains belonging to a given cation were treated as independent

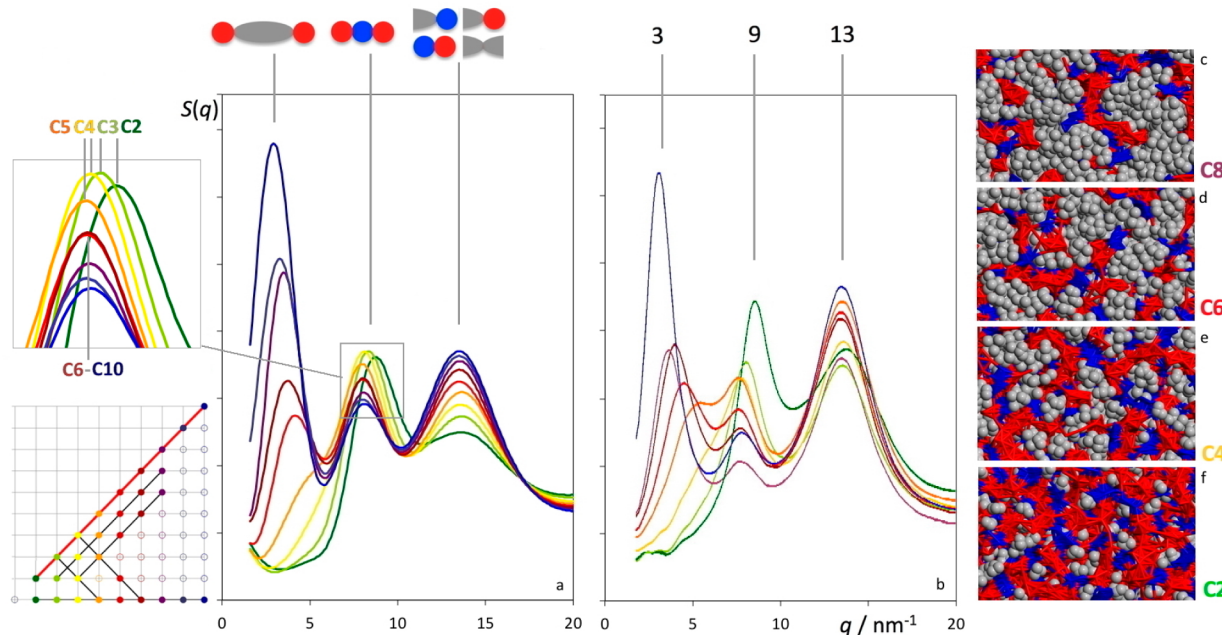


Figure 1. Structure factors, $S(q)$, as a function of the reciprocal space wavenumber, q , for the $[C_nC_m\text{im}][\text{Ntf}_2]$ ($m = n$) homologous series. The colors of each particular system ($S(q)$ lines, legend for panels c–f) are coded according to Scheme 1. The inset at the bottom left identifies (red line) the systems/series under discussion (cf. Scheme 1). (a) MD simulation data (this work); (b) representation based on the X-ray data from Rocha et al.³² The simulation snapshots (c–f) are color coded to reflect the presence of the charged parts of the cations (blue), the anions (red), and the two alkyl side chains (tails) of the cations (gray). The small vignettes above (a) represent structural features assigned to each peak (see text); the numbers above (b) indicate the approximate q values (in nm^{-1}) of each family of peaks.

units. This means that alkyl-tail aggregates that are connected only via “ionic bridges” are to be considered distinct nonpolar domains.

Finally, several statistical functions were used to characterize the network/aggregates that emerge from the connectivity lists.^{19,29} These include (i) $P(n_a)$, the probability distribution function of finding an ionic moiety or alkyl side chain in an aggregate of a given size (with n_a ionic moieties or alkyl side chains); (ii) N_b , the average number of first-contact neighbors of a given ionic moiety (ionic moieties of opposite charge) or alkyl side chain (other alkyl side chains); (iii) $N_i(n_a)$, the average number of neighbors within an aggregate of size n_a ; (iv) $R_d(n_a)$, the average ratio of the longest distance between two atoms belonging to the same aggregate of size n_a to the simulation box diagonal; and (v) $R_V(n_a)$, the ratio of the apparent volume of an aggregate of size n_a to the volume of the simulation box. These five statistical tools have been introduced and described in more detail elsewhere.¹⁹

RESULTS AND DISCUSSION

Structure Factors. Figures 1–3 show the structure-factor functions obtained using MD simulations of the five IL series analyzed in this work.

As mentioned in the Introduction, the structure factors of the $[C_nC_m\text{im}][\text{Ntf}_2]$ series have been studied by other authors (both experimentally and via modeling methods).^{5,18,30–32} Recently the experimental studies have been extended to the $[C_nC_m\text{im}][\text{Ntf}_2]$ ($m = n$) series, where both alkyl side chains have the same length.³²

Figure 1a,b compares MD results obtained in this work with experimental X-ray diffraction data.³² The two plots are accompanied by four simulation snapshots (panels c–f) showing the progressive “growth” and segregation of the

nonpolar domains as the two alkyl side chains of the cations become longer along the homologous series. Figures 2 and 3 show only MD results since there is no available experimental data.

It must be stressed that the intensity scale of the $S(q)$ plots is arbitrary and that no $S(q)$ data is available for $q < 1.6 \text{ nm}^{-1}$; even with relatively large simulation boxes, the corresponding boundary conditions introduce spurious effects below that

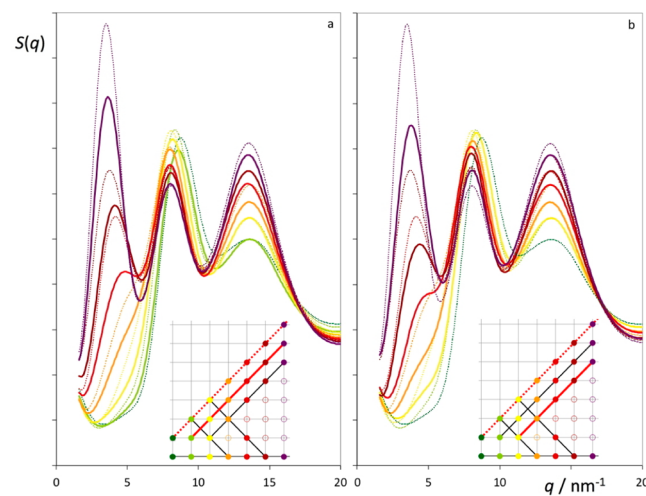


Figure 2. Structure factors, $S(q)$, as a function of the reciprocal space wavenumber, q , for the (a) $[C_nC_m\text{im}][\text{Ntf}_2]$ ($m = n - 1$) and (b) $[C_nC_m\text{im}][\text{Ntf}_2]$ ($m = n - 2$) homologous series. The colors of each particular system ($S(q)$ lines) are coded according to Scheme 1. The insets in (a) and (b) identify (red lines) the systems/series under discussion (truncated versions of Scheme 1). The dashed lines correspond to the spectra presented in Figure 1a.

threshold. Nevertheless, the trends, namely, the peak q values and their intensity shifts along the series, are quite similar between the MD and experimental data (Figure 1). Such was also the case for the previously studied $[C_nC_1\text{im}][\text{Ntf}_2]$ series.¹⁹

The spectra are characterized by the existence of three q -value ranges where the so-called low- q peaks can be found: (i) 13, (ii) 8–9 (intermediate peaks), and (iii) 2–5 nm⁻¹ (prepeaks). These peaks are the sum of different contributions from intra- and intermolecular pair correlation functions with different signs and amplitudes. This means that in a liquid it is always difficult to assign a peak to a characteristic distance between a particular pair of atomic centers and also to describe the relative intensities and trends between peaks, including the appearance of shoulders or other less conspicuous features.

Nevertheless, as one moves along the different members of a given series, the intensities of the three sets of peaks generally shift in a regular manner, for both the MD and X-ray results, and it is therefore possible to infer some structural features that can then be confirmed by further structural analyses (see next sections). In this context, the three sets have been associated^{5,19} with length scales assigned to (i) direct contact pairs between the charged parts of the anions and cations, (ii) the closest distances between ions of the same sign within the polar network, and (iii) ion–ion distances mediated by nonpolar domains; see the vignettes on top of Figure 1a, where the blue circles represent the charged part of the cations (the imidazolium rings plus the atoms directly attached to them), the red circles represent the anions, and the gray ellipsoids represent the alkyl side chains of the cations, from C2 to CT, cf. Scheme 1).

One of the most conspicuous trends is that of the so-called prepeaks that can be found (or not) in the 2–5 nm⁻¹ region.

In Figure 1, one can see that from $[C_2C_2\text{im}][\text{Ntf}_2]$ to $[C_4C_4\text{im}][\text{Ntf}_2]$ this peak is not present (or is a very tenuous shoulder/perturbation of the intermediate peaks centered at 8–9 nm⁻¹); for $[C_5C_5\text{im}][\text{Ntf}_2]$, the simulation data shows a shoulder and the X-ray diffraction data shows a small peak centered at around 5 nm⁻¹ (still partially merged with the intermediate peak); and from $[C_6C_6\text{im}][\text{Ntf}_2]$ onward, one has increasingly more intense peaks shifted progressively toward lower q values.

As in the case of the $[C_nC_1\text{im}][\text{Ntf}_2]$ series (single tails), the development and shift of the prepeaks along the $[C_nC_m\text{im}][\text{Ntf}_2]$ ($m = n$) (symmetrical tails) series can be associated with the emergence of larger and bulkier nonpolar domains that can form a bicontinuous mesoscopic phase for ILs with longer alkyl side chains. In the case of the single-tail series, the percolation of the isolated nonpolar domains found for the C2–C4 members of the series into a continuous nonpolar subphase occurred around C5; in the case of the symmetrical-tails series, we will see later that the percolation event occurs earlier in the series (C3) but the corresponding continuous subphase is not bulky enough to allow the development of a prepeak that is sufficiently intense or differentiated from the intermediate peak. The present study shows that the percolation of a continuous nonpolar subphase is a necessary but not sufficient condition for the appearance of distinct and intense prepeaks. The bulkiness of the nonpolar subphase also plays a role, but apparently only when the alkyl side chains contained in the nonpolar subphase are larger than pentyl is it possible to observe the corresponding prepeaks. A case in point is the data for $[C_5C_5\text{im}][\text{Ntf}_2]$ that shows a prepeak at around 5 nm⁻¹ that is still partially merged with the intermediate peak.

This also means that the shift of the prepeak to smaller q values (corresponding to larger distances in normal space) as the alkyl side chains increase in length is strongly associated with the increase in bulkiness (width) of the nonpolar subphases, which in turn will separate more effectively different strands of the polar network: the prepeaks develop due to intense and noncanceling correlations between atoms included in such polar network strands (e.g., the heavier sulfur atoms contained in the anions will contribute disproportionately to the X-ray diffraction patterns).

Figure 2 shows the structure factors of ILs with two long alkyl side chains that are no longer symmetrical. (One side chain is one methylene group shorter than the other in Figure 2a and two methylene groups shorter than the other in Figure 2b.) The structure factors from the symmetrical case were also superimposed in the two figures to allow comparisons between them. In the case of Figure 2a, one sees that the six prepeaks of the asymmetrical-tails series (solid lines) are intercalated with the seven prepeaks of the symmetrical-tails series (dotted lines). This makes sense since the nonpolar domains formed by ionic liquids with, for instance, C5–C6 tails should present a bulkiness somewhere in between the values of those formed by ILs with C6–C6 and C5–C5 tails. Using the same type of argument, in the case of Figure 2b, an ionic liquid with C4–C6 tails should exhibit a prepeak region similar to that of C5–C5. However, that is not completely true: the asymmetric peaks tend to be slightly more intense than in the corresponding symmetrical case, emphasizing that the length of the longest tail will dictate most of the effect (the size and width of the nonpolar domains) and not just the average of the two tails.

Such a state of affairs can be seen in a clearer way if we compare the series where the total number of carbon atoms in both tails is kept constant (Figure 3a with $n + m = 6$ and Figure 3b with $n + m = 8$). In this case, we see quite clearly that as one of the tails gets longer and the other one gets shorter, the

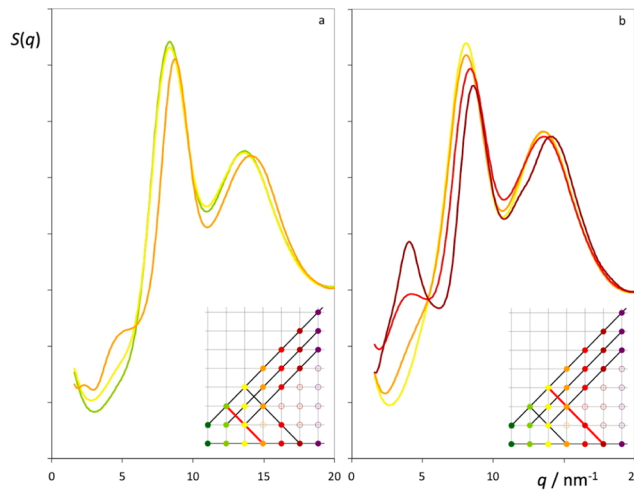


Figure 3. Structure factors, $S(q)$, as a function of the reciprocal space wavenumber, q , for the (a) $[C_nC_m\text{im}][\text{Ntf}_2]$ ($m + n = 6$) and (b) $[C_nC_m\text{im}][\text{Ntf}_2]$ ($m + n = 8$) homologous series. The colors of each particular system ($S(q)$ lines) are coded according to Scheme 1. The insets in (a) and (b) identify (red lines) the systems/series under discussion (truncated versions of Scheme 1). The dashed lines correspond to the spectra presented in Figure 1a and are given for comparison purposes.

prepeaks become more intense as a response to the existence of one longer side chain.

The second q region to be addressed is that centered around 9 nm^{-1} , which is where the so-called intermediate peaks are to be found. In Figures 1 and 2 (where the chains grow along the series), the intermediate peaks are characterized by decreasing intensities along the series (opposite trends relative to those of the prepeaks) and small shifts toward lower q values (trends similar to those observed for the prepeaks). As mentioned before for the single-tail systems,¹⁹ these results—weaker correlations and slightly larger characteristic distances between ions of the same sign within the polar network as the alkyl side chains become longer—are consistent with the fact that the polar network must be partially broken in order to accommodate progressively larger nonpolar domains. This will have an impact on the number of counterions present in the first shell of a given ion (cf. aggregate analyses below) and an even larger effect on the number of second-shell (same-charge) ions and can explain the intensity decrease of the intermediate peak along the series.

On the other hand, the gradual transformation of the polar network, from a more or less isotropic/globular arrangement (cf. Figure 1f for $[\text{C}_2\text{C}_2\text{im}][\text{Ntf}_2]$) to a bicontinuous structure with a more stringlike and stretched polar network (cf. Figure 1c for $[\text{C}_8\text{C}_8\text{im}][\text{Ntf}_2]$), can explain the shifts of the intermediate peak to smaller q values (cf. inset of Figure 1a). Such shifts are very pronounced from C2 to C3 (start of the formation of large aggregates) and from C3 to C4 (percolation threshold) and less so from C4 to C5. However, the shifts are almost null above C6 (fully stretched polar network). This means that before C5–C6 the polar network is being deformed by the growth and coalescence of the nonpolar aggregates in its midst, but from C6 onward, the growth of the nonpolar regions mainly causes an increase in the distances between different strands of the polar network (appearance of a distinct prepeak and its shift to lower q values). It is remarkable that such a minimum critical alkyl length (CAL) associated with a C5–C6 alkyl side chain (0.7 – 0.8 nm between the centroid of the imidazolium ring and the terminal carbon atom of the chain)²⁶ is quite close to the characteristic length of the stretched polar network (8.1 nm^{-1} corresponds to a spacing of 0.77 nm between ions of the same charge in direct space). One can surmise that only when the alkyl side chains grow longer than the sphere of influence of the polar network (literally and figuratively speaking, cf. Figure 4) can they actually start to separate the different polar strands of the network effectively and not just sheath them.

Radial Distribution Functions. The presence of a continuous polar network throughout the different homologous series—a hallmark of ionic liquids attested to by the persistence of the intermediate $S(q)$ peaks just discussed—can also be analyzed in direct space using the corresponding ion–counterion and ion–ion radial distribution functions (RDFs). These are presented in Figure 5 for seven selected ionic liquids belonging to two different homologous series (the symmetrical tails and $n + m = 8$ cases).

The periodic behavior of the RDFs presented if Figure 5 can be regarded as the “fingerprint” of the polar network of the ionic liquids: the need to fulfill local electroneutrality conditions implies the existence of first-shell neighbors of opposite charge (gray lines with a first peak at ionic contact distances) surrounded by second-shell neighbors of similar charge (blue and red lines with a first peak in the first valley of

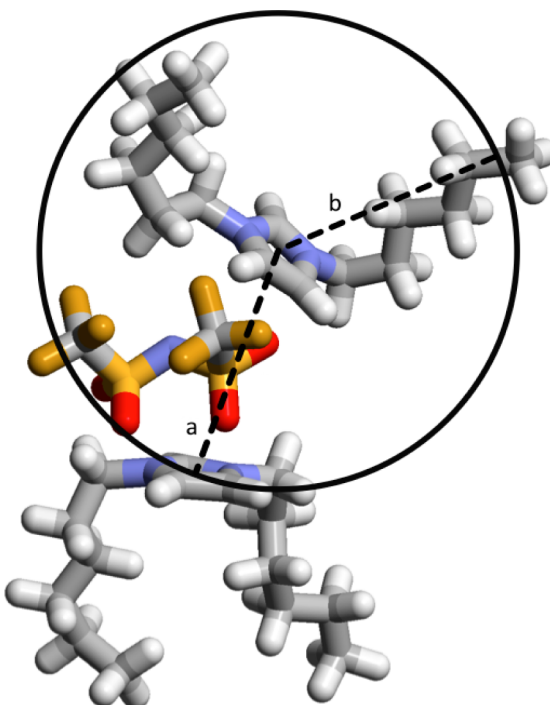


Figure 4. Similarity between the characteristic wavelength of the polar network (a: distance between ions of the same sign) and the minimal critical alkyl length, CAL, of the longest chain in a $[\text{C}_n\text{C}_m\text{im}]^+$ cation (b: distance between the imidazolium ring centroid and a position in the chain between C5 and C6). The represented ions were selected from a configuration of a simulation run of $[\text{C}_6\text{C}_6\text{im}][\text{Ntf}_2]$.

the gray lines). Depending on the nature of the ions, this arrangement can be further propagated at longer distances, and the resulting medium-range periodical ordering (opposition of phase between the RDFs) is translated in reciprocal space as the intermediate q peaks.

In the case of the $[\text{C}_n\text{C}_m\text{im}][\text{Ntf}_2]$ ($m = n$) series (Figure 5a–d), the use of large simulation boxes (cubic boxes with sides greater than 10 nm) allowed the extension of the RDF length limits up to more than 5 nm. In the case of $[\text{C}_2\text{C}_2\text{im}][\text{Ntf}_2]$ (Figure 5a), the periodicity of the RDFs allows the identification of up to 10 shells of alternating charge surrounding a particular ion. The periodicity becomes less conspicuous as one move along the series (which explains the decrease in intensity of the corresponding intermediate q peaks). Nevertheless, even in the case of $[\text{C}_8\text{C}_8\text{im}][\text{Ntf}_2]$ (Figure 5d) one can easily count seven to eight surrounding shells. It must be stressed that the spacing of the grids along the series ($\Delta d = 0.722, 0.776, 0.785$, and 0.780 nm from $[\text{C}_2\text{C}_2\text{im}][\text{Ntf}_2]$ to $[\text{C}_8\text{C}_8\text{im}][\text{Ntf}_2]$) was calculated from the positions of the q peaks ($q = 8.7, 8.1, 8.0$, and 8.1 nm^{-1}) using the relation $\Delta d = 2\pi/q$. The grid lines show that as the nonpolar domains increase in size along the series, the polar network will persist but will have to accommodate the growing nonpolar domains by losing part of its connectivity (and becoming more disordered at longer distances) but also by slightly stretching itself (ionic layers with greater wavelength values, intermediate peak shifts to smaller q values). In this context, one can speculate that the existence of large and flexible anions such as $[\text{Ntf}_2]^-$ or cations with charge-delocalized rings such as $[\text{C}_n\text{C}_1\text{im}]^+$ can play an important role in such stretching-without-rupture processes: as the polar network swells, the ions can adopt different conformations or

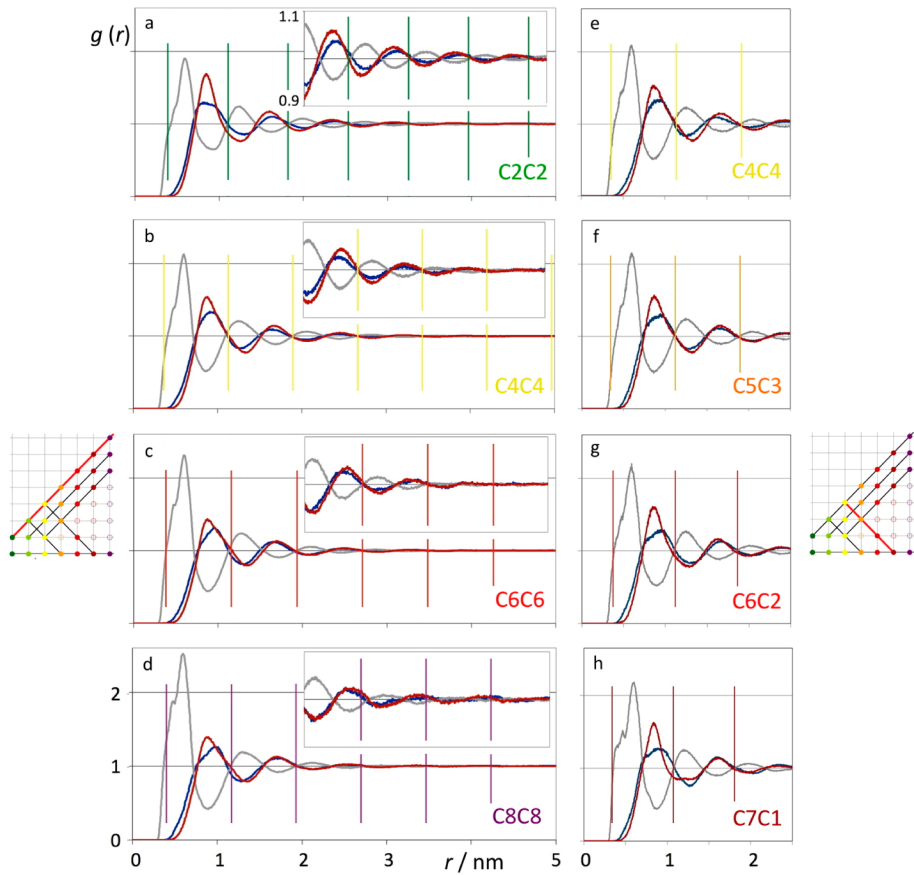


Figure 5. Selected radial distribution functions (RDFs), $g(r)$, as a function of distance, r , for seven ionic liquids in the (a–d) $[C_nC_m\text{im}][\text{Ntf}_2]$ ($m = n$) and (e–h) $[C_nC_m\text{im}][\text{Ntf}_2]$ ($n + m = 8$) series. Gray lines: RDFs between the imidazolium ring centroid (cation) and the NBT atom of the anion (cf. Scheme 1). Blue lines: cation–cation RDFs. Red lines: anion–anion RDFs. The colored vertical lines reflect the periodicity of the RDFs (wavelength) and were calculated from the q values of the corresponding intermediate q peaks in Figures 1a and 3b. The insets in a–d magnify the region between 2 and 5 nm vertically. The two small schematic insets on the sides show the relations (red lines) between the series under discussion (truncated versions of Scheme 1).

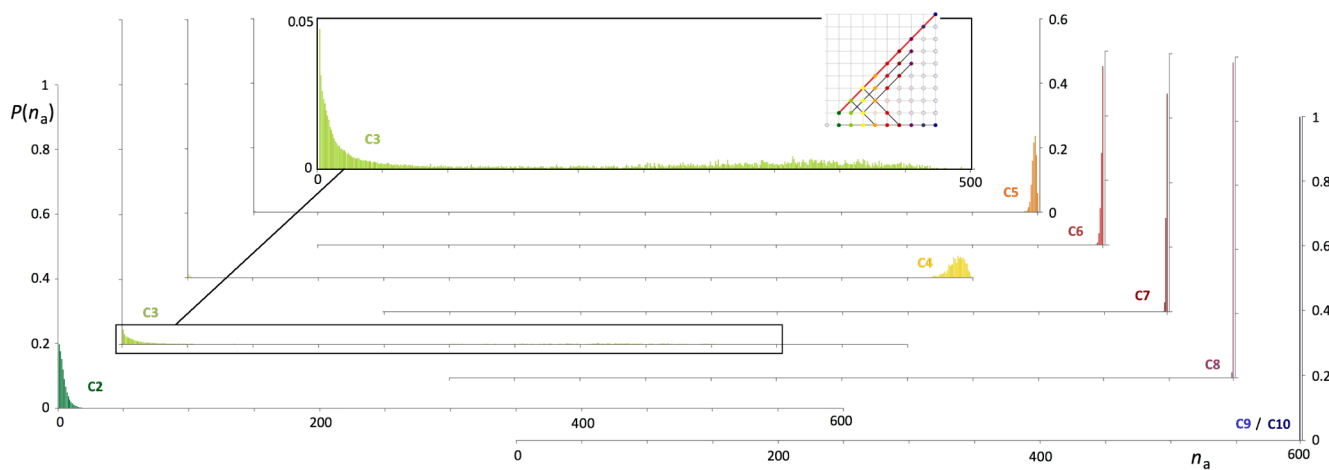


Figure 6. Discrete probability distribution functions of nonpolar aggregate sizes, $P(n_a)$, as a function of the aggregate size number, n_a , for the $[C_nC_m\text{im}][\text{Ntf}_2]$ ($m = n$) series. The small schematic inset shows the series (red line) under discussion (cf. Scheme 1).

relative configurations that enable them to interact equally well with different counterions at slightly longer distances. It is also interesting that the largest “stretch” occurs between $[C_2C_2\text{im}][\text{Ntf}_2]$ and $[C_4C_4\text{im}][\text{Ntf}_2]$, when (as we will see in the next section) the nonpolar domains start to form a second continuous subphase.

In the case of the $[C_nC_m\text{im}][\text{Ntf}_2]$ ($n + m = 8$) series (Figure 5e–h), the volume occupied by the nonpolar domains is more or less constant, but their distribution around the polar network is not. As the two tails become less symmetrical, the grid spacing tends to decrease ($\Delta d = 0.776, 0.776, 0.748$, and 0.731 nm from $[C_4C_4\text{im}][\text{Ntf}_2]$ to $[C_7C_1\text{im}][\text{Ntf}_2]$), which corroborates the formation of a second continuous subphase.

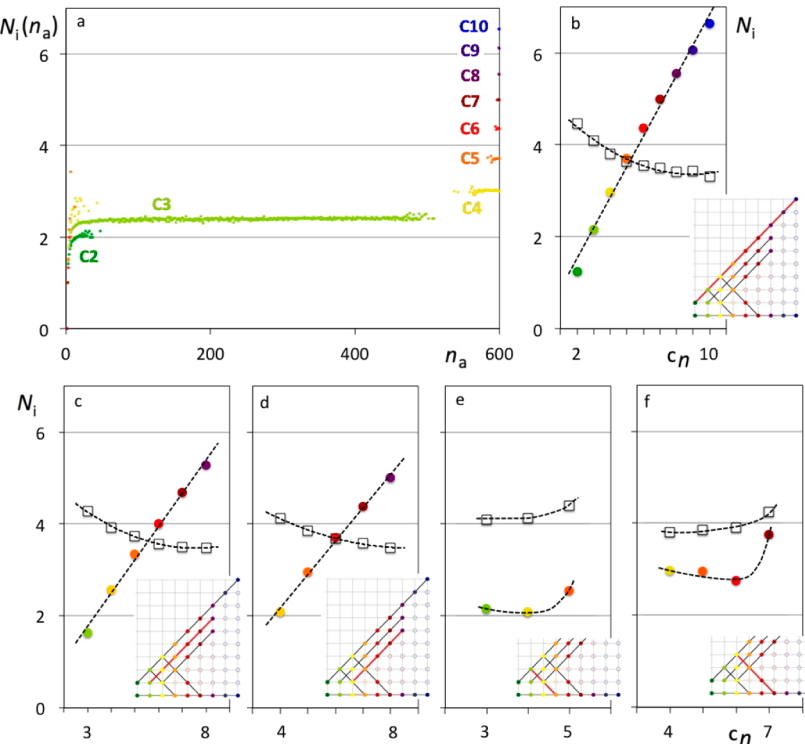


Figure 7. (a) Number of contact neighbors, $N_i(n_a)$, as a function of the aggregate size number, n_a , for tail aggregates in the $[C_nC_m\text{im}][\text{Ntf}_2]$ ($m = n$) series. (b–f) Average size of contact neighbors, N_i , in the polar network (empty squares) or in the tail aggregates (filled color circles) as a function of the alkyl side chain length, C_n , for (b) $[C_nC_m\text{im}][\text{Ntf}_2]$ ($m = n$), (c) $[C_nC_{m-1}\text{im}][\text{Ntf}_2]$ ($m = n - 1$), (d) $[C_nC_{m-2}\text{im}][\text{Ntf}_2]$ ($m = n - 2$), (e) $[C_nC_{m-3}\text{im}][\text{Ntf}_2]$ ($n + m = 6$), and (f) $[C_nC_{m-4}\text{im}][\text{Ntf}_2]$ ($n + m = 8$). The five small schematic insets show the relations (red lines) between the series under discussion (truncated versions of Scheme 1).

brates the increase in the q values of the corresponding intermediate q peaks ($q = 8.1, 8.1, 8.4$, and 8.6 nm^{-1}). Since the nonpolar parts of the alkyl side chains only start at C2, one can speculate that the charged part of the $[C_7C_1\text{im}]^+$ cations can adopt more conformations within the polar network than their more symmetrically substituted counterparts and that the segregation between the nonpolar domains and the polar network is more efficient when the polar head of the cation is not constrained by the existence of two quasisymmetrical alkyl side chains. Both factors point to a less stretched polar network for ionic liquids composed of asymmetrical side chains, especially for the $[C_nC_1\text{im}][\text{Ntf}_2]$ cases.

Aggregate Analysis. In this section we will use the different statistical tools introduced in the Experimental Section to analyze the aggregation patterns that emerge within the different $[C_nC_m\text{im}][\text{Ntf}_2]$ series. The simulation boxes used to calculate the trajectories to be analyzed contained 300 ion pairs and 600 alkyl side chains. This means that the corresponding distribution analyses as a function of the number of ions or tails belonging to a given aggregate (n_a) will always range from 0 to 600.

Figure 6 shows the probability distribution function of nonpolar aggregate sizes, $P(n_a)$, along the $[C_nC_m\text{im}][\text{Ntf}_2]$ ($m = n$) series.

Before discussing the $P(n_a)$ functions for the nonpolar aggregates, one must make a reference to the analogous functions for the polar network. The calculation of $P(n_a)$ for the ionic part of all ionic liquids under discussion has yielded $P(1) \approx P(2) \approx \dots \approx P(599) \approx 0$ and $P(600) \approx 1$. This confirms that even for $[C_{10}C_{10}\text{im}][\text{Ntf}_2]$, a given ion is always part of an aggregate that contains all other ions present in the simulation

box (i.e., there are no isolated fragments of the polar network). Such a large aggregate is the polar network. This is in agreement with energy-minimization arguments that prevent the existence of isolated ions or ion pairs (electrostatic dipoles) in the midst of nonpolar entities such as aliphatic chains.

The $P(n_a)$ functions for the nonpolar (tail) aggregates exhibit completely different behavior, with high probabilities of small aggregates for cations with very short tails, high probabilities of all-encompassing (continuous) aggregates for the largest members of the series, and polydisperse distributions for systems near the continuous to bicontinuous percolation limit. Figure 6 shows only the results for the symmetrical-tails series, but the situation is very similar for all other cases.

In $[C_2C_2\text{im}][\text{Ntf}_2]$, some 20% of the chains (in this case, just the terminal CH_3 group of the ethyl chain) are isolated in the midst of the polar network, some 18% of them are paired, 15% form trios, and very few aggregate “islands” with more than 10 tails were observed. As one progresses from $[C_2C_2\text{im}][\text{Ntf}_2]$ to $[C_3C_3\text{im}][\text{Ntf}_2]$, the distribution undergoes a very noticeable shift: even though the most probable occurrence is still the existence of isolated tails (5%), there are now non-negligible probabilities of finding aggregates that include almost all tails (there is a broad secondary probability distribution with a maximum around $n_a = 370$, cf. inset in Figure 6). This means that the percolation limit that marks the transition to a continuous nonpolar subphase has almost been reached. This kind of behavior has already been observed for the single-tail $[C_nC_1\text{im}][\text{Ntf}_2]$ series, but such a percolation limit was attained only after $[C_5C_1\text{im}][\text{Ntf}_2]$. Of course the volumes occupied by the nonpolar domains in $[C_3C_3\text{im}][\text{Ntf}_2]$ and $[C_5C_1\text{im}][\text{Ntf}_2]$ are very similar, which means that such a volume fraction is

somehow connected to the formation of the nonpolar continuous subphase. The most interesting fact, though, is that in the present case such percolation is not accompanied by the appearance of a prepeak in the corresponding structure factors; it starts to appear (as in the case of the single-tail series) only around the ionic liquids with five carbon atoms in their alkyl side chains. It must also be stressed that none of the aggregates observed in $[C_3C_3\text{im}][\text{Ntf}_2]$ comprise all of the chains contained in the simulation box and that most of the time a majority of the aggregates are not able to percolate the entire simulation box, although, being very large clusters, they are still not able to form a second continuous mesophase (cf. discussion of the size and shape of the aggregates below).

The rest of the members of $[C_nC_m\text{im}][\text{Ntf}_2]$ ($m = n$) show very large aggregates that contain most of the tails. (From time to time a few tails separate from the main cluster and form small satellite aggregates.) These large aggregates percolate the entire simulation box most of the time. Such behavior (all-encompassing aggregates, full percolation) becomes more notorious for the $[C_7C_7\text{im}][\text{Ntf}_2]$ to $[C_{10}C_{10}\text{im}][\text{Ntf}_2]$ ionic liquids.

The next parameter to be considered is the number of neighbors of a given ion or tail. This can be calculated as a function of the aggregate size that contains a given ion or tail, $N_i(n_a)$, or as a function of the average number for the entire simulation box, N_i . Figure 7 represents N_i for all studied ILs (ion and tail neighbors) and $N_i(n_a)$ for the $[C_nC_m\text{im}][\text{Ntf}_2]$ ($m = n$) series (tail neighbors).

For the polar network, the total number of neighbors N_i (Figure 7b, empty squares) varies between a bit above 4.5 (for $[C_2C_2\text{im}][\text{Ntf}_2]$) and 3.4 (for $[C_{10}C_{10}\text{im}][\text{Ntf}_2]$). The N_i values decrease in a regular decaylike fashion along the series and seem to decrease more slowly for the largest members of the series. These results are consistent with the progressive swelling and partial breakdown of the polar network as it tries to accommodate progressively larger nonpolar domains. If one compares the symmetrical $[C_nC_m\text{im}][\text{Ntf}_2]$ ($m = n$) with the single-tail $[C_nC_1\text{im}][\text{Ntf}_2]$ series,¹⁹ then the former has a smaller number of neighbors (4.5 to 3.4) than the latter (5.0 to 4.0). This fact can be reconciled if one notices that the cation charged part is less hindered in the single-tail series than in the symmetrical-tail series. For all other series (Figure 7c–f, empty squares), the N_i values for the polar network vary around an average number of 4.0, consistent with the trends observed for the symmetrical series. These trends (Figures 7b–d, empty squares)—faster decrease in the number of neighbors for the members of the series up to C5/C6 followed by a more subdued (stationary) regime after such a critical alkyl length, CAL, is attained—are also in agreement with the rationalization inferred by Figure 4, supporting the previous interpretation of the experimental thermophysical results done by Rocha et al.^{32–35}

The increasing number of neighbors along the series with a constant number of carbon atoms in the alkyl side chains (Figure 7e,f) is also consistent with less-hindered charged moieties for the progressively more asymmetrical cations (especially the large increases for $[C_5C_1\text{im}][\text{Ntf}_2]$ and $[C_7C_1\text{im}][\text{Ntf}_2]$).

In the case of tail aggregates, one can conduct a much richer neighbor analysis based on the number of contact neighbors as a function of the aggregate size number, $N_i(n_a)$.

For $[C_2C_2\text{im}][\text{Ntf}_2]$, the number of neighbors of a given tail varies between 0 (20% of the tails are isolated) to around 2

when the tail is incorporated into small aggregates with a few (up to around 20) other tails (cf. C2 data in Figure 7a). The corresponding N_i value is around 1.2 (C2 point in Figure 7b) and represents the average of $N_i(n_a)$ weighted by the aggregate distribution. The relatively small number of neighbors (never much greater than 2) even in aggregates with around 10 tails or more means that the tails in those aggregates are grouped side by side rather than arranged in a more bundlelike and interconnected way.

For the $[C_3C_3\text{im}][\text{Ntf}_2]$ case, the aggregate size distribution is much broader (still below but quite near the percolation limit) and the number of neighbors is fairly constant and slightly above 2 for aggregates with sizes between 10 and 500 (cf. C3 data in Figure 7a). These rather low contact neighbor numbers (a given tail is surrounded by just two or three other tails in aggregates that may contain tens or hundreds of other tails) indicate once again a more side-to-side arrangement of the tails within the aggregates. This also suggests that such aggregates should be elongated rather than globular (interconnected).

For the rest of the series, the aggregate distribution starts to favor large aggregates that consolidate most of the tails present in the simulation box, and the average number of neighbors will lie very close to the average number of aggregates found on those aggregates (cf. Figure 7a,b). Such numbers of neighbors increase in an extremely regular fashion from $[C_4C_4\text{im}][\text{Ntf}_2]$ (three neighbors) to $[C_{10}C_{10}\text{im}][\text{Ntf}_2]$ (almost seven neighbors). The increasing N_i value reflects on one hand the fact that longer tails can have more contact neighbors simply because they are longer and there are more possible contact points along the length of the chain. On the other hand, as the nonpolar domains start to get larger, the side-by-side orientation that is favored in the smaller elongated aggregates can be extended in more than one direction after the percolation limit is achieved: side-by-side tails in one dimension (row) means two neighbors per tail; side-by-side tails in two dimensions can easily mean six neighbors; three-dimensional globular bundles where the chains can be intertwined with each other can have more than six neighbors.

One important fact to notice is that the neighbor data for the symmetrical-tail $[C_nC_m\text{im}][\text{Ntf}_2]$ ($m = n$) series (1.2 to 6.6 neighbors in the $n = 2$ to 10 range) is higher than the corresponding values for the single-tail $[C_nC_1\text{im}][\text{Ntf}_2]$ series (0.8 to 5.3 neighbors in the $n = 2$ to 10 range). However, the differences do not fully take into account the fact that for a given n the volume occupied by the nonpolar domains is much larger (more or less than double) in the $[C_nC_m\text{im}][\text{Ntf}_2]$ ($m = n$) series than in the $[C_nC_1\text{im}][\text{Ntf}_2]$ series. For instance, $[C_4C_4\text{im}][\text{Ntf}_2]$ and $[C_7C_1\text{im}][\text{Ntf}_2]$ must have similar volume fractions occupied by the tail domains, but the number of neighbors in $[C_4C_4\text{im}][\text{Ntf}_2]$ (3 neighbors) is smaller than that in $[C_7C_1\text{im}][\text{Ntf}_2]$ (3.8 neighbors). This suggest that having two half tails is not as efficient in the promotion of bulky nonpolar domains as having a single tail with double the length (which agrees with the structure factor data, e.g., Figure 3b). It also indicates that in terms of the definition of the prepeaks the length of the longest peak is an important issue.

The relative ability of single-tailed cations and their polytailed counterparts (e.g., tetra-alkyl ammonium cations) to generate (or not) well-segregated bulky nonpolar domains and the corresponding prepeaks has been discussed recently in different papers.^{19,36} When a single long alkyl chain is substituted by many smaller chains (with a combined number

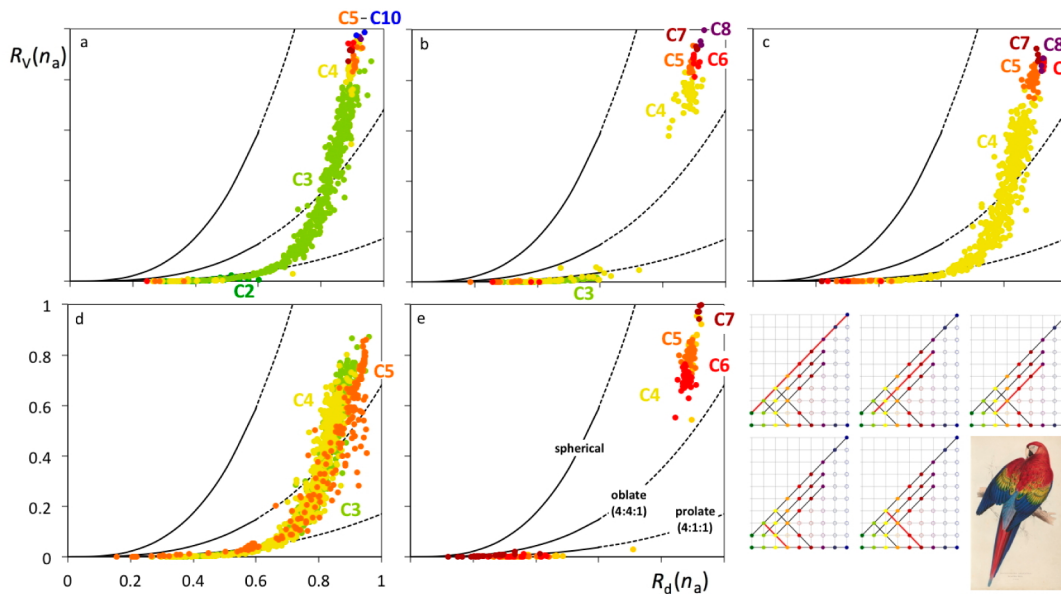


Figure 8. (Aggregate volume)-to-(box volume) ratio, $R_V(n_a)$, as a function of (aggregate maximum length)-to-(box diagonal) ratio, $R_d(n_a)$, for all tail aggregates in the studied $[C_nC_m\text{im}][\text{Ntf}_2]$ homologous series. (a) $[C_nC_m\text{im}][\text{Ntf}_2]$ ($m = n$), (b) $[C_nC_m\text{im}][\text{Ntf}_2]$ ($m = n - 1$), (c) $[C_nC_m\text{im}][\text{Ntf}_2]$ ($m = n - 2$), (d) $[C_nC_m\text{im}][\text{Ntf}_2]$ ($n + m = 6$), and (e) $[C_nC_m\text{im}][\text{Ntf}_2]$ ($n + m = 8$). The five small schematic insets show the relations (red lines) between the series under discussion (truncated versions of Scheme 1). The lithograph of a scarlet macaw³⁷ refers to both the different color schemes used to depict the different series and the existence of different colored data “tails”.

of carbons that can even exceed that of the single chain), there is a sheathing effect of the polar network by elongated nonpolar domains that preclude the neat segregation of bulky nonpolar regions and the existence of strong prepeaks.³⁶ The same happens when a single long alkyl chain is substituted by a single chain of the same size that can interact more strongly with the polar network and sheath it (e.g., a glycol ether chain).

The final set of parameters to be investigated is related to the length and volume of the aggregates as a function of their size, namely, the ratios between those two quantities and the length of the diagonal of the cubic box and its volume, $R_d(n_a)$ and $R_V(n_a)$. Since the polar network percolates the entire simulation boxes for all studied series, the determination of $R_d(n_a)$ and $R_V(n_a)$ only makes sense for the tail aggregates. Figure 8 shows $R_V(n_a)$ as a function of $R_d(n_a)$ (panel c) for each $[C_nC_m\text{im}][\text{Ntf}_2]$ ($m = n$) series.

Since the distribution of tail aggregates along any of the series is never uniform— $[C_2C_2\text{im}][\text{Ntf}_2]$ and other members of the series with very small alkyl side chains form only small islandlike aggregates with relatively small n_a values; those with larger tails form percolating aggregates containing all or almost all tails in the simulation box ($n_a \approx 600$)—the $R_V(n_a)$ and $R_d(n_a)$ functions will never be complete for a given ionic liquid. However, it is possible to obtain useful information if one plots $R_V(n_a)$ versus $R_d(n_a)$ along the entire series and observes the trends that emerge from the combination of data from the different members of the series.

Figure 8a shows that for small aggregates (corresponding to n_a = up to 50 tails) their lengths increase more rapidly than their volumes when more tails are added to the aggregate (the points of Figure 8a stay close the x axis). This means that smaller aggregates tend to be elongated, which corroborates the number of neighbors data. In fact, the volume-to-length ratio trend for those small aggregates lies close to that of a prolate ellipsoid with 4:1:1 axes ratios (depicted in the figure).

As aggregates become larger (as one moves along the series beyond $[C_3C_3\text{im}][\text{Ntf}_2]$), their volumes R_V start to increase more rapidly, and the volume-to-length ratio trend inflects upward. This means that for larger aggregates ($n_a > 50$) the arrangement of the tails inside the aggregates starts to be more interconnected, with more than 2 neighboring tails per tail, and the shape of the aggregate moves from prolate-like objects to more oblate-like ones.

It must be stressed at this point that the trends depicted in Figure 8 representing the volume-to-length ratios in spheroid objects (black lines denoting spheres and ellipsoids) are just guidelines to help understand the approximate shapes of the aggregates with a given $R_d(n_a)$ to $R_V(n_a)$ relation. The 1:4 ratio between the main axes of the oblate and prolate ellipsoids was empirically selected in order to have a match between the shape of prolate ellipsoids and the $R_d(n_a)$ and $R_V(n_a)$ data for aggregates with $n_a < 50$. Moreover, the black lines for the spheroid objects become dotted at a maximum length value of $(1/3)^{(1/2)} \approx 0.6$. This value marks the point at which the maximum length of the spheroid objects reaches the size of the side of the simulation box. While the volume-to-length ratios of the spheroids can still be calculated beyond this point, their comparison to $R_d(n_a)$ and $R_V(n_a)$ values must be progressively more cautious simply because the volume of aggregates will be limited by the boundary conditions imposed by the simulation box itself.

Figure 8b,c shows the trends in the $[C_nC_m\text{im}][\text{Ntf}_2]$ ($m = n - 1$) and $[C_nC_m\text{im}][\text{Ntf}_2]$ ($m = n - 2$) series. One interesting point to observe is that as one of the chains get slightly smaller (and the volume fraction occupied by the tail domains decreases), the start of the percolation threshold (as attested by the inflection in the volume-to-ratio trends and the existence of data for aggregates of intermediate size) increases from $n = 3$ (cf. the green data “tail” of $[C_3C_3\text{im}][\text{Ntf}_2]$ in Figure 8a) to something between 3 and 4 (the green $[C_3C_2\text{im}][\text{Ntf}_2]$ data in Figure 8b shifts to small aggregates but the yellow $[C_4C_3\text{im}][\text{Ntf}_2]$

$[\text{Ntf}_2]$ data still does not cover all aggregate sizes), to $n = 4$ (the yellow “tail” data of $[\text{C}_4\text{C}_2\text{im}][\text{Ntf}_2]$ in Figure 8c). This is consistent with the facts that $[\text{C}_3\text{C}_3\text{im}][\text{Ntf}_2]$ and $[\text{C}_4\text{C}_2\text{im}][\text{Ntf}_2]$ tails occupy similar volume fractions and that in both cases the average number of neighbors just exceeds 2 (Figure 7b,d).

Figure 8d highlights this point more vividly: in the case of systems $[\text{C}_n\text{C}_m\text{im}][\text{Ntf}_2]$ ($n + m = 6$) all members of the series ($[\text{C}_3\text{C}_3\text{im}][\text{Ntf}_2]$, $[\text{C}_4\text{C}_2\text{im}][\text{Ntf}_2]$, and $[\text{C}_5\text{C}_1\text{im}][\text{Ntf}_2]$) are near the onset of the percolation and the corresponding volume-to-length graphs show three colored data “tails” with $n = 3, 4$, and 5 . On the other hand, the $[\text{C}_n\text{C}_m\text{im}][\text{Ntf}_2]$ ($n + m = 8$) series are all past the percolation threshold, and no data can be obtained for aggregates of intermediate sizes.

The exuberance of colors and the use of the word “tails” in the context of both tail aggregates and data tails led us to introduce in Figure 8 the drawing of a scarlet macaw (*Ara macao*) by Edward Lear.³⁷ The image also suggests the importance of analyzing structural trends along different homologous series, as depicted by the small inset schemes introduced in the different figures and also insinuated by the succession of colors along the wings and body of the macaw.

CONCLUSIONS

This systematic study tried to interpret different aspects related to the mesoscopic structure of five $[\text{C}_n\text{C}_m\text{im}][\text{Ntf}_2]$ homologous series, including ionic liquids with symmetrically alkyl-substituted cations.

The trajectories obtained in MD simulations of neat ionic liquids belonging to those series were used to calculate the corresponding $g(r)$ and $S(q)$ functions, and the results enabled us to rationalize and confirm the relation between the existence of a low- q $S(q)$ prepeak and the formation of a continuous well-segregated and bulky nonpolar subphase when the length of the longest alkyl side chain of the cation exceeds or is around 5. The structural changes that occur in the polar network along the series were also considered, taking into account the trends observed for the low- q $S(q)$ intermediate peak and its correspondence to the spacing between polar network shells in the corresponding $g(r)$ functions.

The structural investigation of the $[\text{C}_n\text{C}_m\text{im}][\text{Ntf}_2]$ systems was then extended to include connectivity and aggregate analyses. These revealed that the percolation of islandlike nonpolar domains (formed by the alkyl side chains of the cations) into a continuous nonpolar subphase occurs when the volume fraction occupied by the tails reaches a given threshold value that corresponds to a total number of carbon atoms in the alkyl side chains, $n + m = 6$, and the average number of direct tail neighbors exceeds 2. This means (unlike hitherto assumed) that percolation is a necessary but not sufficient condition for prepeak emergence. Other aggregate analyses (aggregate distribution, number of neighbors in the polar network and in the tail aggregates, and aggregate shape) yielded consistent results throughout the different homologous series. These provide a coherent framework for future discussions on the molecular level of the complex mesoscopic structure of the physical–chemistry properties and application of ionic liquids.

ASSOCIATED CONTENT

Supporting Information

Enlarged version of Figures 1–3 and 6 in the main text. Schematic representation of the five statistical functions that were used in the aggregate analyses of the MD data IL

homologous series. This material is available free of charge via the Internet at <http://pubs.acs.org>.

AUTHOR INFORMATION

Corresponding Author

*E-mail: jnlopes@ist.utl.pt.

Author Contributions

K.S. and C.E.S.B. contributed equally to this work as first authors.

Notes

The authors declare no competing financial interest.

ACKNOWLEDGMENTS

Financial support was provided by Fundação para a Ciência e Tecnologia (FCT) through projects FCT-ANR/CTM-NAN/0135/2012 (including a postdoctoral grant to K.S.), PTDC/CTM-NAN/121274/2010, PEst-C/QUI/UI0081/2013, and PEst-OE/QUI/UI0100/2013. C.E.S.B. and A.I.M.C.L.F. acknowledge postdoctoral grants SFRH/BPD/43346/2008 and SFRH/BPD/84891/2012, respectively.

REFERENCES

- (1) Urahata, S. M.; Ribeiro, M. C. C. Structure of Ionic Liquids of 1-Alkyl-3-Methylimidazolium Cations: A Systematic Computer Simulation Study. *J. Chem. Phys.* **2004**, *120*, 1855–1863.
- (2) Wang, Y.; Voth, G. A. Unique Spatial Heterogeneity in Ionic Liquids. *J. Am. Chem. Soc.* **2005**, *127*, 12192–12193.
- (3) Pádua, A. A. H.; Canongia Lopes, J. N. Nanostructural Organization in Ionic Liquids. *J. Phys. Chem. B* **2006**, *110*, 3330–3335.
- (4) Triolo, A.; Russina, O.; Bleif, H.; Di Cola, E. Nanoscale Segregation in Room Temperature Ionic Liquids. *J. Phys. Chem. B* **2007**, *111*, 4641–4644.
- (5) Annareddy, H. V. R.; Kashyap, H. K.; De Biase, P. M.; Margulis, C. J. What is the Origin of the Prepeak in the X-ray Scattering of Imidazolium-Based Room-Temperature Ionic Liquids? *J. Phys. Chem. B* **2010**, *114*, 16838–16846.
- (6) Bhargava, B. L.; Devane, R.; Klein, M. L.; Balasubramanian, S. Nanoscale Organization in Room Temperature Ionic Liquids: A Coarse Grained Molecular Dynamics Simulation Study. *Soft Matter* **2007**, *3*, 1395–1400.
- (7) Castner, E. W.; Wishart, J. F. Spotlight on Ionic Liquids. *J. Chem. Phys.* **2010**, *132*, 120901–1–120901–9.
- (8) Hardacre, C.; Holbrey, J. D.; Mullan, C. L.; Youngs, T. G. A.; Bowron, D. T. Small Angle Neutron Scattering from 1-Alkyl-3-methylimidazolium Hexafluorophosphate Ionic Liquids ($[\text{C}_n\text{min}][\text{PF}_6]$, $n = 4, 6$, and 8). *J. Chem. Phys.* **2010**, *133*, 74510–74517.
- (9) Kashyap, H. K.; Santos, C. S.; Sanjeeva Murthy, N.; Hettige, J. J.; Kerr, K.; Ramati, S.; Gwon, J.; Gohdo, M.; Lall-Ramnarine, S. I.; Wishart, J. F.; Margulis, C. J.; Castner, E. W. Structure of 1-Alkyl-1-Methylpyrrolidinium Bis(trifluoromethylsulfonyl)amide Ionic Liquids with Linear, Branched, and Cyclic Alkyl Groups. *J. Phys. Chem. B* **2013**, *117*, 15328–15337.
- (10) Kashyap, H. K.; Hettige, J. J.; Annareddy, H. V. R.; Margulis, C. J. SAXS Anti-Peaks Reveal the Length-Scales of Dual Positive–Negative and Polar–Apoliar Ordering in Room-Temperature Ionic Liquids. *Chem. Commun.* **2012**, *48*, 5103–5105.
- (11) Borodin, O.; Smith, G. D. Structure and Dynamics of N-Methyl-N-propylpyrrolidinium Bis(trifluoromethanesulfonyl)imide Ionic Liquid from Molecular Dynamics Simulations. *J. Phys. Chem. B* **2006**, *110*, 11481–11490.
- (12) Siqueira, L. J. A.; Ribeiro, M. C. C. Charge Ordering and Intermediate Range Order in Ammonium Ionic Liquids. *J. Chem. Phys.* **2011**, *135*, 204506–1–204506–7.
- (13) Yamaguchi, T.; Mikawa, K.; Koda, S.; Fujii, K.; Endo, H.; Shibayama, M.; Hamano, H.; Umebayashi, Y. Relationship Between

- Mesoscale Dynamics and Shear Relaxation of Ionic Liquids With Long Alkyl Chain. *J. Chem. Phys.* **2012**, *137*, 104511–1–104511–7.
- (14) Borodin, O.; Gorecki, W.; Smith, G. D.; Armand, M. Molecular Dynamics Simulation and Pulsed-Field Gradient NMR Studies of Bis(fluorosulfonyl)imide (FSI) and Bis[(trifluoromethyl)sulfonyl]imide (TFSI)-Based Ionic Liquids. *J. Phys. Chem. B* **2010**, *114*, 6786–6798.
- (15) Gontrani, L.; Russina, O.; Lo Celso, F.; Caminiti, R.; Annat, G.; Triolo, A. Liquid Structure of Trihexyltetradecylphosphonium Chloride at Ambient Temperature: An X-ray Scattering and Simulation Study. *J. Phys. Chem. B* **2009**, *113*, 9235–9240.
- (16) Hettige, J. J.; Kashyap, H. K.; Annapureddy, H. V. R.; Margulis, C. J. Anions, the Reporters of Structure in Ionic Liquids. *J. Phys. Chem. Lett.* **2013**, *4*, 105–110.
- (17) Song, X. D.; Hamano, H.; Minofar, B.; Kanzaki, R.; Fujii, K.; Kameda, Y.; Kohara, S.; Watanabe, M.; Ishiguro, S.; Umebayashi, Y. Structural Heterogeneity and Unique Distorted Hydrogen Bonding in Primary Ammonium Nitrate Ionic Liquids Studied by High-Energy X-ray Diffraction Experiments and MD Simulations. *J. Phys. Chem. B* **2012**, *116*, 2801–2813.
- (18) Zheng, W.; Mohammed, A.; Hines, L. G., Jr.; Xiao, D.; Martinez, O. J.; Bartsch, R. A.; Simon, S. L.; Russina, O.; Triolo, A.; Quitevis, E. L. Effect of Cation Symmetry on the Morphology and Physicochemical Properties of Imidazolium Ionic Liquids. *J. Phys. Chem. B* **2011**, *115*, 6572–6584.
- (19) Shimizu, K.; Bernardes, C. E. S.; Canongia Lopes, J. N. Structure and Aggregation in the 1-Alkyl-3-Methylimidazolium Bis(trifluoromethylsulfonyl)imide Ionic Liquid Homologous Series. *J. Phys. Chem. B* **2014**, *118*, 567–576.
- (20) Canongia Lopes, J. N.; Deschamps, J.; Pádua, A. A. H. Modeling Ionic Liquids Using a Systematic All-Atom Force Field. *J. Phys. Chem. B* **2004**, *108*, 2038–2047.
- (21) Canongia Lopes, J. N.; Pádua, A. A. H. Molecular Force Field for Ionic Liquids Composed of Triflate or Bistriflylimide Anions. *J. Phys. Chem. B* **2004**, *108*, 16893–16898.
- (22) Canongia Lopes, J. N.; Pádua, A. A. H. CL&P: A Generic and Systematic Force Field for Ionic Liquids Modeling. *Theor. Chem. Acc.* **2012**, *131*, 1129.
- (23) Jorgensen, W. L.; Maxwell, D. S.; Tirado-Rives, J. Development and Testing of the OPLS All-Atom Force Field on Conformational Energetics and Properties of Organic Liquids. *J. Am. Chem. Soc.* **1996**, *118*, 11225–11236.
- (24) Smith, W.; Forester, T. R. *DL_POLY Package of Molecular Simulation Routines (v.2.2)*; The Council for The Central Laboratory of Research Councils, Daresbury Laboratory: Warrington, U.K., 2006.
- (25) Chandler, D. *Introduction to Modern Statistical Mechanics*; Oxford University Press: New York, 1987; pp195–201.
- (26) Shimizu, K.; Bernardes, C. E. S.; Triolo, A.; Canongia Lopes, J. N. Nano-Segregation in Ionic Liquids: Scorpions and Vanishing Chains. *Phys. Chem. Chem. Phys.* **2013**, *15*, 16256–16262.
- (27) Brown, P. J.; Fox, A. G.; Maslen, E. N.; O’Keefe, M. A.; Willis, T. M. *International Tables for Crystallography*; Prince, E., Ed.; International Union of Crystallography: Dordrecht, The Netherlands, 2004; Vol C, pp 554–595.
- (28) Lorch, E. Neutron Diffraction by Germania, Silica and Radiation-Damaged Silica Glasses. *J. Phys. C: Solid State Phys.* **1969**, *2*, 229–237.
- (29) Bernardes, C. E. S.; Minas da Piedade, M. E.; Canongia Lopes, J. N. The Structure of Aqueous Solutions of a Hydrophilic Ionic Liquid: The Full Concentration Range of 1-Ethyl-3-methylimidazolium Ethylsulfate and Water. *J. Phys. Chem. B* **2011**, *115*, 2067–2074.
- (30) Raju, S. G.; Balasubramanian, S. Role of Cation Symmetry in Intermolecular Structure and Dynamics of Room Temperature Ionic Liquids: Simulation Studies. *J. Phys. Chem. B* **2010**, *114*, 6455–6463.
- (31) Bodo, E.; Gontrani, L.; Caminiti, R.; Plechkova, N. V.; Seddon, K. R.; Triolo, A. Structural Properties of 1-Alkyl-3-methylimidazolium Bis[(trifluoromethyl)sulfonyl]amide Ionic Liquids: X-ray Diffraction Data and Molecular Dynamics Simulations. *J. Phys. Chem. B* **2010**, *114*, 16398–16407.
- (32) Rocha, M. A. A.; Neves, C. M. S. S.; Freire, M. G.; Russina, O.; Triolo, A.; Coutinho, J. A. P.; Santos, L. M. N. B. F. Alkylimidazolium Based Ionic Liquids: Impact of Cation Symmetry on Their Nanoscale Structural Organization. *J. Phys. Chem. B* **2013**, *117*, 10889–10897.
- (33) Rocha, M. A. A.; Lima, C. F. R. A. C.; Gomes, L. R.; Schröder, B.; Coutinho, J. A. P.; Marrucho, I. M.; Esperança, J. M. S. S.; Rebelo, L. P. N.; Shimizu, K.; Canongia Lopes, J. N.; et al. High-Accuracy Vapor Pressure Data of the Extended [CnC1im][Ntf₂] Ionic Liquid Series: Trend Changes and Structural Shifts. *J. Phys. Chem. B* **2011**, *115*, 10919–10926.
- (34) Rocha, M. A. A.; Coutinho, J. A. P.; Santos, L. M. N. B. F. The Cation Symmetry Effect on the Volatility of Ionic Liquids. *J. Phys. Chem. B* **2012**, *116*, 10922–10927.
- (35) Rocha, M. A. A.; Coutinho, J. A. P.; Santos, L. M. N. B. F. Evidence of Nanostructuration from the Heat Capacities of the 1,3-Dialkylimidazolium Bis(trifluoromethylsulfonyl)imide Ionic Liquid Series. *J. Chem. Phys.* **2013**, *139*, 104502.
- (36) Pereiro, A. B.; Gallego, M. J. P.; Shimizu, K.; Marrucho, I. M.; Canongia Lopes, J. N.; Piñeiro, M. M.; Rebelo, L. P. N. On the Formation of a Third, Nanostructured Domain in Ionic Liquids. *J. Phys. Chem. B* **2013**, *117*, 10826–10833.
- (37) Peck, R. M. The Natural History of Edward Lear. *Nature* **2012**, *485*, 36–38.